ENERGY AND THERMAL MODELING OF BUILDING FAÇADE INTEGRATED PHOTOVOLTAICS

by

Konstantinos ORDOUMPOZANIS[a], Theodoros THEODOSIOU[b*], Dimitrios BOURIS[c], and Katerina TSIKALOUDAKI[b]

[a] Department of Mechanical Engineering, University of Western Macedonia, Kozani, Greece
[b] Laboratory of Building Construction and Building Physics, Aristotle University of Thessaloniki, Thessaloniki, Greece
[c] Laboratory of Aerodynamics, School of Mechanical Engineering, National Technical University of Athens, Athens, Greece

Original scientific paper
https://doi.org/10.2298/TSCI170905025O

Electricity generation on site is a design challenge aiming at supporting the concept of energy-autonomous building. Many projects worldwide have promoted the installation of photovoltaic panels on urban buildings, aiming at utilizing a large area to produce electricity. In most cases, photovoltaics are considered strictly as electricity generators, neglecting their effect to the efficiency and to the thermal behaviour of the building envelope. The integrated performance of photovoltaic ventilated façades, where the photovoltaics are regarded as part of a complicated envelope system, provides design challenges and problems that cannot be overlooked within the framework of the Nearly Zero Energy Building concept. In this study, a finite volume model for photovoltaic ventilated façades is developed, experimentally validated and found to have a significant convergence to measured data.

Key words: *photovoltaics, ventilated façade, building envelope, modelling*

Introduction

The recently adopted framework for near Zero Energy Buildings (nZeb) has introduced new challenges regarding not only the energy consumption of buildings but also the energy production through onsite renewable energy sources. To support the effort to conform with the nZeb requirements, a building has not only to reduce the energy consumption but also to produce energy. In cases when these tasks can be integrated in a single system or procedure, then the potential benefits are important. A recent popular way of embedding the photovoltaic (PV) modules is by integrating them on the building's ventilated façades [1]. In such cases, the PV module beyond being an electricity producer, is also an additional external layer forming a double skin façade [2].

Model development

As the actual thermal and energy phenomena of the examined system are quite complicated, simplifications are necessary in order to approach the problem in an efficient way. The main assumptions of the model as explained hereafter, are the fully developed, uniform air cavity flow, the maximum air speed of 5 m/s, the maximum ambient temperature of 60 °C and that the air cavity is vertical.

* Corresponding author, e-mail: tgt@civil.auth.gr

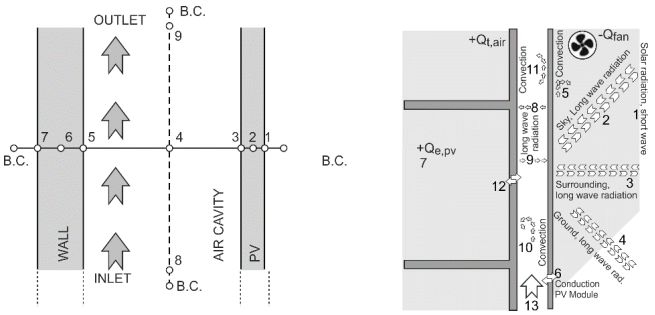

Figure 1. Discretization of the model (left) and physical model of the examined system (right)

Physical model

The first step in the process of modelling the system is the domain discretization in areas having the same physical phenomena. In the examined construction, there are three discrete domains (fig. 1):

– (a) the PV modules where the main physical heat transfer mechanism is the thermal diffusion [9]:

$$\frac{1}{a}\frac{\vartheta U}{\vartheta t}=\frac{\vartheta^2 U}{\vartheta x^2}+\frac{q_i^{'}}{k_i} \tag{1}$$

– (b) The cavity area between the modules and the building's wall where there is mass transfer [10]:

$$K_{i,I}(\xi)=v_{i,I}(\xi)\overline{\rho}_{i,I}(\xi)\overline{C}_{i,I}(\xi) \tag{2}$$

– (c) The back-wall where eq. (1) is also applicable. Each of these three discrete areas is described by three nodes which is the minimum number of required nodes.

The energy balance of the system implements the following heat transfer mechanisms: (1) Solar gain (short-wave radiation gain), (2) long-wave radiation heat transfer between façade and sky, (3) long-wave radiation heat transfer between façade and surrounding surfaces, (4) long-wave radiation heat transfer between façade and ground, (5) convectional heat transfer in the outermost surface of the façade with the ambient air, (6) heat conduction inside the PV panels, (7) electricity production from the PV panels, (8) long-wave radiation heat transfer between the back surface of the PV modules and the back wall, (9) long-wave radiation heat transfer between the wall and the back surface of the PV module, (10) convectional heat transfer between the back surface of the façade and the moving air inside the cavity, (11) convectional heat transfer between the wall and the moving air inside the cavity, (12) conduction heat transfer inside the wall, and (13) mass transfer on the air cavity from inlet to outlet.

Thermal model

The thermal phenomena of the system are highly related to the air speed and to the air temperature within the cavity. For this reason, the properties of the air vary in relation to its temperature. The formulas describing the thermal state of the system are presented hereafter.

Air properties

The air properties at specific temperature K are calculated from the following equations [11]:

$$b_{air}=9.1\cdot10^{-11}T^2+8.8197\cdot10^{-8}T-1.0654\cdot10^{-5} \tag{3}$$

$$v_{air}=-1.1555\cdot10^{-14}T^3+9.5728\cdot10^{-11}T^2+3.7604\cdot10^{-8}T-3.448\cdot10^{-6} \tag{4}$$

$$k_{air}=1.502\cdot10^{-11}T^3-4.8574\cdot10^{-8}T^2+1.0184\cdot10^{-4}T-3.9333\cdot10^{-1} \tag{5}$$

$$e_{air}=1/T \tag{6}$$

$$\rho_{air}=360.77819T^{-1.00336} \tag{7}$$

$$Cp_{air} = 1.9327 \cdot 10^{-10} T^4 - 7.9999 \cdot 10^{-7} T^3 + 1.1407 \cdot 10^{-3} T^2 - 4.4890 \cdot 10^{-1} T + 1.0575 \cdot 10^{3} \quad (8)$$

$$\mathrm{Pr}_{air} = \frac{\nu}{\beta} \quad (9)$$

Sky temperature

The long-wave heat exchange radiation between the façade and the sky has been implemented in the model through the sky temperature [9]:

$$\mathrm{T}_{sky} = \left(e_{sky} T_{dp}^4 \right)^{0.25} - T_{amb} \quad (10)$$

The sky emissivity (ε_{sky}), and the dew point temperature (T_{dp}) are estimated from the Magnus-Tetens formula [12]:

$$\varepsilon_{sky} = \left[0.787 + 0.76 \ln\left(\frac{T_{dp}}{273} \right) \right] \left(1 + 0.224 N_{sky} - 0.0035 N_{sky}^2 + 0.00028 N_{sky}^3 \right) \quad (11)$$

$$T_{dp} = 237.7 \left[\ln\left(\frac{RH}{100} \right) + \frac{17.271 \cdot T_{amb}}{237.7 + T_{amb}} \right] / \left\{ 17.271 - \left[\ln\left(\frac{RH}{100} \right) - \frac{17.271 T_{amb}}{237.7 + T_{amb}} \right] \right\} \quad (12)$$

Long-wave heat transfer

The mechanism of long-wave heat transfer on the outermost surface of the façade is calculated through the Watlon and McClellan & Pedester formula by using an equivalent linearized radiation coefficient hr for each of the three factors (sky, surroundings, ground) [13]:

$$\dot{q_{LWR}} = h_{r,grd} \left(T_{surf} - T_{grd} \right) + h_{r,sky} \left(T_{surf} - T_{sky} \right) + h_{r,air} \left(T_{surf} - T_{amb} \right) \quad (13)$$

$$h_{r,grd} = \frac{\varepsilon \sigma F_{grd} \left(T_{surf}^4 - T_{grd}^4 \right)}{T_{surf} - T_{grd}}, \quad F_{grd} = 0.5 \left(1 - \cos\Phi \right) \quad (14)$$

$$h_{r,sky} = \frac{\varepsilon \sigma F_{sky} \beta \left(T_{surf}^4 - T_{sky}^4 \right)}{T_{surf} - T_{sky}}, \quad \beta = \sqrt{0.5(1 + \cos\Phi}, \quad F_{sky} = 0.5 \left(1 + \cos\Phi \right) \quad (15)$$

$$h_{r,air} = \frac{\varepsilon \sigma F_{sky} \left(1 - \beta \right) \left(T_{surf}^4 - T_{sky}^4 \right)}{T_{surf} - T_{sky}}, \quad \beta = \sqrt{0.5(1 + \cos\Phi}, \quad F_{sky} = 0.5 \left(1 + \cos\Phi \right) \quad (16)$$

Within the cavity the linearized coefficient hr is also used to describe long-wave radiation pahinomena [14]:

$$h_{rad} = 4 \sigma T_m^3 / \left(\frac{1}{\varepsilon_{pv}} + \frac{1}{\varepsilon_{wall}} + 1 \right), \quad T_m = \left(T_{pv} + T_{wall} \right) / 2 \quad (17)$$

In this study, the emissivity of the PV surfaces are: $\varepsilon_{pv,out} = 0.81$, $\varepsilon_{pv,in} = 0.85$ and for the wall $\varepsilon_{wall} = 0.9$ (smooth concrete) [15].

Convection heat transfer on the outermost surface of the façade

Double façades are systems in contact to the ambient air. The interior air flow is a very complicated phenomenon, as it depends on the geometry and the air characteristics. To enhance

calculation speed and result's accuracy, the presented model implements an average analytical expression of the convection heat transfer coefficient, proposed for thermal solar collector's usage [16, 17]:

$$h_{c,out} = 5.74 u_{air}^{4/5} H_{pv}^{-1/5} \tag{18}$$

Convection inside the façade

The presented convection coefficients derive from literature, and have been collected for creating a model with extended operational and geometrical limits. In all cases, the convection coefficient is calculated from an average Nusselt number [16]:

$$h_c = \mathrm{Nu} k_{air} / L_{\mathrm{Nu}} \tag{19}$$

The flow characteristics of the convection coefficient varies, according to the operational and geometrical characteristic of the façade. In the model, the assumption of a fully developed flow within the air cavity is made. Based on this assumption, the state of the flow is calculated (free, forced, or in between state) and for each of these states an additional calculation identifies the nature of flow like laminar, turbulent or transient.

Air flow

Archimedes number characterizes the flow's main force [16]:

$$\mathrm{Ar} \quad \mathrm{Gr}/\mathrm{Re} \tag{20}$$

where Ar ≥ 4.0 for free flow, Ar ≤ 0.25 for forced flow and 0.25 < Ar < 4.0 for intermediate case. Two more dimensional numbers are required for the calculation of Ar. The Reynolds (Re) number and the Grashof (Gr) number:

$$\mathrm{Re} = u_{air,gap} L_{Re} / V_{air} \tag{21}$$

$$\mathrm{Gr} = g\beta \left(T_{surf} - T_{air} \right) L_{Gr}^3 / v_{air} \tag{22}$$

In the case of free flow, the main driven force is buoyancy and the characteristic number for this flow type is the Rayleigh number.

$$\mathrm{Ra} = \mathrm{GrPr} \tag{23}$$

For this state, there must be another control regarding the boundary layers of the flow near the solid surfaces. In the case of two separate discrete boundaries that do not affect each other, the air cavity is characterized as *wide*. In the reverse case, it is characterized as *narrow*. Numerically, this check is based on the ratio of façade's length to height as it has been proved elsewhere [17]:

$$\frac{L}{H} > \mathrm{Ra}^{-1/4} \text{ for wide façade, or } \frac{L}{H} < \mathrm{Ra}^{-1/4} \text{ for narrow façade} \tag{24}$$

For each of the two cases, the Ra number indicates if the flow is in laminar or turbulent state [17, 18].

$$10^{l} < \mathrm{Ra} < 10^{9} \quad \text{for laminar flow,} \quad \text{or } 10^{9} < \mathrm{Ra} < 10^{12} \quad \text{for turbulent flow} \tag{25}$$

The wide façade case is described by two Nusselt numbers. The first one applies on Rayleigh number of range $10^{-1} < \mathrm{Ra} < 10^{12}$ [19].

$$\mathrm{Nu} = \left(0.825 + 0.328 \mathrm{Ra}_H^{1/6} \right)^2 \tag{26}$$

For the case of the narrow façade for a uniform heat flow over a plate it becomes [20].

$$\begin{aligned} &\mathrm{Nu}_{L,fd} = 0.29(\mathrm{Ra}(W/H))^{1/2} \\ &\mathrm{Nu}_{L,bl} = 0.67(\mathrm{Ra}(W/H))^{1/5} \\ &\mathrm{Nu}_{L} = (\mathrm{Nu}_{L,fd}^{-3.5} + \mathrm{Nu}_{L,bl}^{-3.5})^{3.5} \\ &\mathrm{Ra}^{W/H} < 10^4 \end{aligned} \tag{27}$$

If the Ra limit of eq. (27) is not valid, then a general heat transfer coefficient for double façades is used for speed limit of 5 m/s inside the façade [21].

$$h_c = 5.23 + 3.9u_{air,gap} \tag{28}$$

Forced air flow

A flow is characterized as *forced* for Ar numbers less than 0.25. In this case, the dimensional number that describes the flow is the Reynolds number [16]:

$$\begin{gathered} \mathrm{Re} < 2300 \text{ for laminar, } \mathrm{Re} > 4000 \text{ for turbulent and} \\ 2300 < \mathrm{Re} < 4000 \text{ for transient flow} \end{gathered} \tag{29}$$

The case of laminar flow, is modelled as flow within a cylindrical pipe with an equivalent hydraulic diameter and the Nusselt number is constant and equal to 4.36 [21]. For the turbulent conditions (Re > 4000) there are two Nusselt correlations. The first one applies in the regime of 4000 <Re ≤ 10^6, known as the Gnielinski formula [22]:

$$\mathrm{Nu}_d = \left((f/2)(\mathrm{Re}-1000)\mathrm{Pr}\right)/\left(1+12.7(f/2)^{1/2}(\mathrm{Pr}^{2/3}-1)\right) \tag{30}$$

The second, for the regime of Re > 106 and for Prandtl numbers in the range of 0.7 ≤ Pr ≤ 160 the Nusselt number is calculated from eq. (31) [20]:

$$\mathrm{Nu}_D = 0.023\mathrm{Re}_D^{0.8}\mathrm{Pr}^{0.4} \tag{31}$$

Finally, for the transitional flows, the Nusselt number is calculated from [23]:

$$\begin{aligned} &\mathrm{Nu}^{10} = \mathrm{Nu}_f^{10} + \left\{ \frac{exp\left[(2200-\mathrm{Re})/365\right]}{\mathrm{Nu}_t} + \frac{1}{\mathrm{Nu}_t^2} \right\}^{-5} \\ &\mathrm{Nu}_f = \mathrm{Nu}_0 + \frac{0.079(f/2)^{1/2}\,\mathrm{RePr}}{\left(1+\mathrm{Pr}^{4/5}\right)^{5/6}} \\ &\mathrm{Nu}_t = 4.364,\ q = \mathrm{const},\ \mathrm{Nu}_0 = 3.60,\ q = \mathrm{const} \end{aligned} \tag{32}$$

Free and forced air flow combination

In most cases of a hybrid ventilated façade, the flow is not completely free or forced and the heat transfer coefficient is calculated in three stages: (a) as a complete free flow, (b) as a complete forced flow, and (c) as a combination of the two previous states, which is finally added to the calculations of the energy balance [21]:

$$\mathrm{hc}_{tot} = \sqrt{hc_{free}^{\ 4} + hc_{forced}^{\ 4}}^{1/4} \tag{33}$$

Friction factor

All model surfaces are considered as *smooth*. This assumption is required for the friction factor calculation. The model has a common algorithm of friction factor calculation for all the states of forced convection. For Re < 2300, the friction is not affected by the pipe roughness [21] and the friction factor depends only on the Reynold number [23]:

$$f = 64/\mathrm{Re} \tag{34}$$

for the transient flow, the friction factor is calculated from the Bhatti and Shah formula [23]:

$$f = 0.0054 + \frac{2.3\cdot 10^{-8}}{\mathrm{Re}^{-3/2}} \tag{35}$$

finally, the turbulent area friction factor is related to the relative roughness of the pipe [24]:

$$k_{\mathrm{pipe}} = \frac{e}{d_{\mathrm{pipe}}} \tag{36}$$

The roughness of the PV module's back surface is considered as smooth glass, equal to $e_{\mathrm{pv}} = 0.0015\cdot 10^{-3}$ m and for the wall (smooth concrete) $e_{\mathrm{wall}} = 1\cdot 10^{-3}$ m. The friction factor for this case is calculated from the Haaland formula [22] and with friction factor known, the pressure drop in the façade can be calculated by applying the Colebrook formula [16]:

$$\frac{1}{f^{1/2}} \approx -1.8\log\left[\frac{6.8}{\mathrm{Re}_D} + \left(\frac{e/D}{3.7}\right)^{1.11}\right] \tag{37}$$

$$\Delta P_f = \frac{fH}{D_h}\frac{\rho u_{air,duct}^2}{2} \tag{38}$$

Closed air cavity

During the operation of a double ventilated façade, there are conditions where ventilation should be avoided to prevent unnecessary thermal losses, like during winter nights. In such cases, a simple automation system could control the inlet and outlets to resist cold ambient air entering the air cavity. For these cases the model incorporates Nusselt number correlations for natural convection on a closed cavity. The calculation of the Nusselt number depends on some dimensional ratios for the façade. If $H/W > 10$ and $10^3 < \mathrm{Ra_w} < 10^7$ [19] the Nusselt number is calculated from the following equation:

$$\mathrm{Nu}_{W90} = \max\left\{\mathrm{Nu}_1, \mathrm{Nu}_2, \mathrm{Nu}_3\right\}, \qquad \mathrm{Nu}_1 = 0.0605\mathrm{Ra}_W^{1/3}$$
$$\mathrm{Nu}_2 = \left\{1 + \left[\frac{0.104\mathrm{Ra}_w^{0.293}}{1+\left(6310/\mathrm{Ra}_w\right)^{1.36}}\right]^3\right\}^{1/3}, \qquad \mathrm{Nu}_3 = 0.242\left(\frac{\mathrm{Ra_w}}{H/W}\right)^{0.272} \tag{39}$$

In the above equation, the characteristic length for the calculation of the Rayleigh number is the width of the cavity. For the same ratio H/W but for smaller Ra numbers, the main heat transfer mechanism is conduction and in this case Nu = 1. For ratio values $10 > H/W \geq 1$ the Nusselt number is calculated as two separate plates geometry in a vertical orthogonal section [25]:

$$\mathrm{Nu} = 0.364\frac{L}{H}\mathrm{Ra}_H^{1/4} \tag{40}$$

For all other cases, literature does not provide adequate formulas, and an analytical expression for a vertical closed cavity is adopted [25].

$$\begin{aligned} \mathrm{Nu}_{90} &= 0.0673838\mathrm{Ra}^{1/3}, \ \ \mathrm{Ra} > 5\times10^{4} \\ \mathrm{Nu}_{90} &= 0.028154\mathrm{Ra}^{0.4134}, \ \ 10^{4} < \mathrm{Ra} \le 5\cdot10^{4} \\ \mathrm{Nu}_{90} &= 1+1.75697\cdot10^{-10}, \ \ \mathrm{Ra} < 10^{4} \end{aligned} \tag{41}$$

Electrical model

The PV electrical characteristics are modelled with an equivalent electrical model of four parameters [9]. This model has been chosen due to its enhanced accuracy and due to the fact that all required input data are usually provided by PV module manufactures' technical description sheets. It calculates the Current-Voltage (I-V) curve for each time step and through it, it can calculate the electrical power production. The model was refined following corrections from [9]:

$$I = I_L - I_0\left\{\exp\left[\frac{q_e V}{\gamma k T_{pv}}\left(V + IR_s\right)\right]\right\} \tag{42}$$

$$I_0 = I_{sc}\exp\left(-\Lambda V_{oc}\right) \tag{43}$$

$$R_S = -M\frac{I_{SC}}{I_{MP}} + \frac{V_{MP}}{I_{MP}}\left(1 - \frac{I_{SC}}{I_{MP}}\right) \tag{44}$$

$$\Lambda = \frac{\dfrac{I_{sc}}{I_{sc} - I_{mp}} + \ln\left(1 - \dfrac{I_{MP}}{I_{sc}}\right)}{2V_{MP} - V_{OC}} \tag{45}$$

$$I_L = I_{SC} \tag{46}$$

$$\gamma = \frac{q_e}{\Lambda k T_{pv}} \tag{47}$$

$$M = \frac{V_{OC}}{I_{SC}}\left(k_1\frac{I_{MP}V_{MP}}{I_{SC}V_{OC}} + k_2\frac{V_{MP}}{V_{OC}} + k_3\frac{I_{MP}}{I_{SC}} + k_4\right) \tag{48}$$

$$k_1 = -5.411, \ \ k_2 = 6.450, \ \ k_3 = 3.417, \ \ k_4 = -4.422 \tag{49}$$

The four-parameter electrical model can give results only for the reference conditions of the module's datasheet. To acquire reliable results for each temperature and solar radiation range, the following corrections should be implemented [25]:

$$a = \frac{\gamma k T_{pv}}{q} \tag{50}$$

$$\frac{a}{a_{ref}} = \frac{T_{pv}}{T_{pv,ref}} \tag{51}$$

$$\frac{\mathrm{I}_o}{\mathrm{I}_{0,ref}} = \left(\frac{T_{pv}}{T_{pv,ref}}\right)^3 \mathrm{e}^{\frac{eN_s}{a_{ref}}\left(1 - \frac{T_{pv,ref}}{T_{pv}}\right)} \tag{52}$$

$$\mathrm{I}_L = \frac{G_{eff}M_{am}}{G_{eff,ref}M_{am,ref}}\left[I_{L,ref} + \alpha_{1_{SC}}\left(T_{pv} - T_{pv,ref}\right)\right] \tag{53}$$

$$\frac{G_{eff}}{G_{eff,ref}} = \frac{\frac{a_{ref}}{I_{o,ref}} e^{\frac{-\left(V_{MP,ref} + I_{MP,ref} R_{s,ref}\right)}{a_{ref}}} + R_s}{\frac{a}{I_0} e^{\frac{-\left(V_{mp} + I_{mp} R_s\right)}{a}} + R_s} \tag{54}$$

$$I_{mp} = I_{mp,ref} \frac{G_{eff}}{G_{eff,ref}} \tag{55}$$

$$V_{mp} = V_{mp,ref} + \beta_{Voc}\left(T_{pv} - T_{pv,ref}\right) \tag{56}$$

The corrections of the above variables are applied in each time step of calculations by using the iterating Newton-Raphson method.

Integration of thermal and electrical models

The two models are integrated within the thermal model in the middle node of the PV module, node 2. The process is the following.

– At the beginning of the time step, the electrical model calculates the electrical production of the PV modules. The PV temperature, which is required for the calculations, is the second node's temperature of the thermal model that corresponds to the mid node of the PV.
– This electrical power of the first step is added to the energy balance of thermal model on node 2 as an output of the system.
– Finally, the new temperature is provided as a feedback to the electrical model and a new corrected power production is calculated. This ping-pong procedure is repeated in the same time step until a convergence limit is reached. The presented model has been programmed on FORTRAN language and has been implemented on the TRNSYS simulation package. The computational solution is based on the methodology that is presented by [7] through finite element analysis in one dimension. According to this methodology and based on the energy conservation law, the energy storage rate in a finite volume should be equal to the total energy rate that come through this finite volume:

$$Q_s = \frac{\rho_I(\xi) C_I(\xi) \delta V_i(\xi)}{dt}\left[\theta(\mathrm{I}, t+\delta t) - \theta(\mathrm{I}, t)\right] = \sum_{j=1}^{N} K_{j,I}\left(\theta_j - \theta_\mathrm{I}\right)\Big|_{t=\xi} + q_I\Big|_{t=\xi} \tag{57}$$

The model, consists of three discrete areas with three nodes each (fig.1). Each node is based on the Crank-Nicolson scheme and is analysed in an implicit and in an explicit time that are joined [16].

Finally, the system to be solved is a 9×9 system. The coefficients A, B, and C are calculated from the physical model.

Boundary conditions

Four boundary conditions are required to solve the system. These are:

– *First node* (*outermost PV's surface*): the boundary condition in this node sets the ambient air node's (outside of the systems boundary) temperature as given and equal to the temperature of the meteorological file.
– *Seventh's node boundary condition*: the room's air temperature (outside of the system boundaries) is a known temperature the can be received from the TRNSYS Building program.

– *Eight's node boundary condition* (*air inlet*): the air temperature that is entering the air cavity is known and its value is equal either to the ambient air or to another known temperature that can be inserted by the TRNSYS simulation program, in case some other air loop is required.
– *Ninth's node temperature* (*outlet*)*:* this is the only boundary condition that needs to be calculated because the outlet temperature is not known. For the proposed model after some test on boundary conditions, it has been found that the energy conservation law can solve this problem:

$$\left.\frac{\partial q}{\partial x}\right|_{n,n+1} = \left.\frac{\partial q}{\partial x}\right|_{n-1,n} + q_{pv,n} \tag{58}$$

This boundary condition states the fact that the energy that leaves from the system is equal to the energy transferred from the eight node to the ninth (due to mass conservation law) plus the energy that is added to the ninth node from the PV and the wall. The numerical solution of this system has some stability problems due to the different magnitudes of coefficients A, B, and C between the solid and fluid layers. In addition, it was found that the boundary conditions, especially on the air inlet and outlet nodes, that are critical for the system solution. The final solution of this system is reached by using the LU decomposition method, which has been proved to be a stable method for all examined cases.

Experimental set-up

To support the development and the evaluation of the model, an experimental set-up of two, hybrid ventilated, opaque, PV façades has been constructed at UWM. These real scale façades are exposed in ambient air and operate in real conditions. The dimension of each test set-up is 1.2 × 2.5 m height and the width can vary from 0.1-0.5 m to allow for testing different flow states.

In these two experimental façades, two different PV module technologies have been implemented (monocrystalline and polycrystalline), both of the same size. In each part of the façade, one air inlet of 0.8 m × 1.2 m is located at the bottom and one outlet is placed at the top of the wall side with dimensions 0.2 m × 1.2 m. The outlet is attached to a converging nozzle followed by a 1.5 m of DN14 pipe with a fan at the end of it (one for each façade). Three surface temperature sensors on each side of each PV module is placed at the top, mid and bottom, and one on each solid wall. An air temperature and air humidity sensor (Hobo 12bit Smart Sensor S-TMB-M002) with accuracy of ±0.2 °C, 2.5%, is placed at the inlet and at the outlet nozzle. Two hot-wire sensors (Delta ohm HD403TD) for air speed recording, one at the end of each pipe with accuracy ±0.2 m/s, and two pyranometers (SKS 1110, horizontal and vertical) measure the incident solar radiation with accuracy 5%. Next to the experimental façades, a meteorological station provides wind data, while each PV's voltage and total current are recorded via Texas Instrument sensors (type NI-SCC-A10, accuracy 0.14%). Air temperature sensors are connected to a Hobo H22 Energy Data Logger, and the rest of sensors to a DL2e Data logger that store data values on a time step of one to five minutes.

Figure 2. Experimental set-up of double, hybrid ventilated, opaque, PV façade

To estimate the measurement error, an analysis of the measured data is applied according to *ASHRAE guideline 2-2010* methodology for sample size less than 30. The analysis results show that the error on each PV surface temperature is about 0.619 °C, 0.437 °C, and 0.629 °C for each position of a PV module (bottom, middle, top) while for the air temperature the error is about 0.956 °C and for the air speed measurements the error is about 0.016 m/s and 0.041 m/s for the monocrystalline and polycrystalline modules, respectively.

Results

The presented results are driven from the comparison of the measured experimental data and the simulation of the TRNSYS implemented model. Results shows that the model approximates very well the physical behaviour of a double, hybrid, ventilated, opaque, façade.

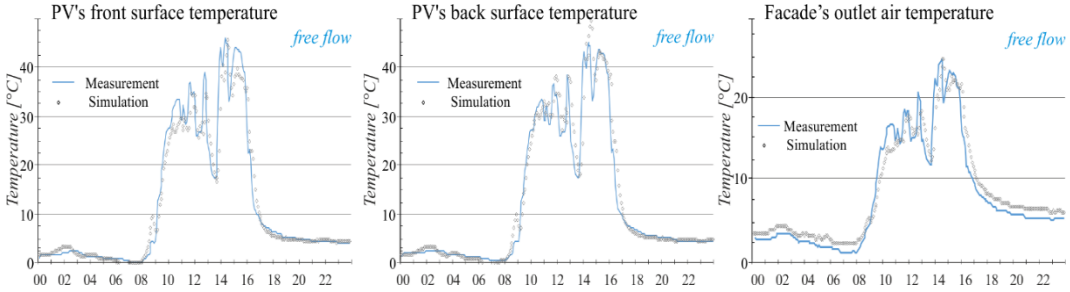

Figure 3. Comparison of measured and simulation results, free flow (6 < Ar < 140)

Figures 3 and 4 present a good accuracy of the model's results to the measured data. For the free flow cases, the results are less accurate than the forced or between states. This was expected due to the simplicity of modelling the free flow conditions in one dimension when the real problem has a much more complicated flow field and a strong buoyancy effect.

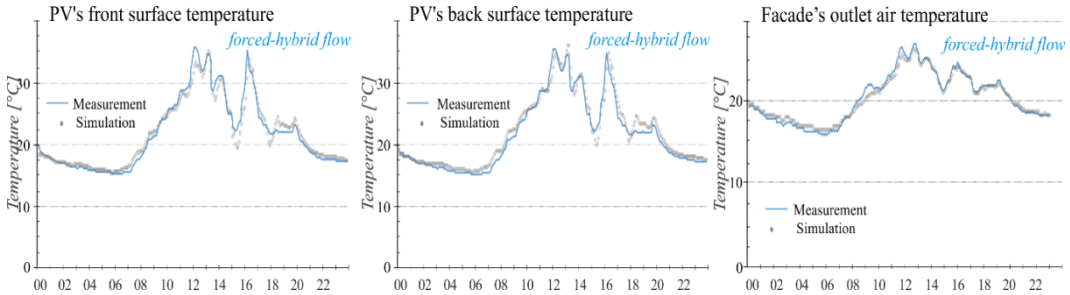

Figure 4. Comparison of measured and simulation results, forced-hybrid flow (0.05 < Ar < 1.1)

Conclusions

The present work analyses the physical mechanisms of a double hybrid ventilated opaque PV façade and proposes a simulation model aiming at predicting accurately the overall energy efficiency of the system, including energy production, thermal behaviour and transient interaction with the building envelope. The model can assist in optimising the design of similar constructions, by studying the interaction of the façade system and the building.

The main difference of this model, when compared to others found in literature, is the computation of the convection coefficients in the air cavity. The calculations are made by dif-

ferent heat transfer coefficient formulas depending on the state of the flow. Another difference is the iterative way of the electrical production through the 4-parameter equivalent model that allows for the estimation of the electricity production in relation to the technical characteristics of the module in each time step.

The accuracy of the model is evaluated by a full-scale experiment exposed to ambient conditions. Regarding surface temperatures, the accurancy is close to 0.6 °C, while for air temperature at the oulet of the system accurncy is slightly less that 1 °C. Better accurancy is achieved for the speed of the extracted air where the error is lower that 0.5 °C. The comparison of the model results with the experimental data shows that the model can efficiently predict the overall thermal behaviour of the system, especially in cases of forced or in between airflow states. In free flow state the model can still provide acceptable results but tends to overestimate the PV's outer surface temperature.

Nomenclature

Ar – Archimedes number, [–]
e_{pv} – roughness of PV module, [m]
e_{wall} – roughness of wall, [m]
f – friction factor, [–]
F – view factor, [–]
G_{eff} – solar radiation, [Wm^{-2}]
Gr – Grashof number, [–]
H – high of façade, [m]
h_c – convection coefficient, [Wm^{-2}K^{-1}]
I – electrical current, [A]
I_{MP} – electrical current at maximum power point of PV module, [A]
I_{SC} – short-circuit electrical current, [A]
k – Stefan-Boltzmann constant (= 1.38066E^{-23}), [J molecule^{-1} K^{-1}]
k_{air} – thermal conduction coefficient of air, [Wm^{-1}K^{-1}]
k_{pipe} – relative roughness, [–]
L – length of facade, [m]
N_S – number of PV cells connected in series, [–]
Nu – Nusselt number, [–]
Pr – Prandtle number, [–]
ΔP – pressure drop, [Pa]
q_e – electron charge (= 1.60218E^{-19})
Ra – Rayleigh number, [–]
Re – Reynolds number, [–]
RH – relative humidity of air, [%]
R_S – equivalent resistant in series of PV's, [Ω]
T_{sky} – sky temperature, [K]
T_{air} – air temperature in the facade's cavity, [K]
T_{amb} – ambient air temperature, [K]
T_{grd} – ground temperature, [K]
T_{pv} – PV module temperature, [K]
T_{surf} – surface temperature, [K]
T_{wall} – wall temperature, [K]
V – electrical voltage, [V]
ν_{air} – air kinematic viscosity, [ms^{-1}]
V_{OC} – open-circuit electrical voltage, [V]
V_{MP} – electrical voltage at maximum power point of PV module, [V]
W – width of the air cavity, [m]

Greek symbols

ε_{sky} – sky emissivity coefficient, [–]
$\boldsymbol{\varepsilon_{pv}}$ – PV module emissivity coefficient, [–]
ε_{wall} – back wall emissivity coefficient, [–]
σ – Stefan-Boltzmann constant (= 5.6697E^{-8}), [Wm^{-2}K^{-4}]
Φ – slope of surface, [deg]
ref – reference condition

References

[1] Pantic, L. S., *et al.*, Electrical Energy Generation with Differently Oriented Photovoltaic Modules as Façade Elements, *Thermal Science, 20* (2016), 4, pp. 1377-1386
[2] Andjelkovic, A. S., *et al.*, Double or Single Skin Façade in a Moderate Climate an Energyplus Assessment, *Thermal Science, 20* (2016), Suppl. 5, pp. S1501-S1510
[3] Gratia, E., De Herde, A., Natural Ventilation in a Double-Skin Façade, *Energy Build., 36* (2004), 2, pp. 137-146
[4] Anderson, T. N., *et al.*, Performance of a Building Integrated Photovoltaic/Thermal (BIPVT) Solar Collector, *Sol. Energy*, *83* (2009), 4, pp. 445-455
[5] Dehra, H., A Two Dimensional Thermal Network Model for a Photovoltaic Solar Wall, *Sol. Energy*, *83* (2009), 11, pp. 1933-1942
[6] Infield, D., *et al.*, Thermal Performance Estimation for Ventilated PV Façades, *Sol. Energy*, *76* (2004), 1-3, pp. 93-98

[7] Nizetic, S., *et al.*, Comprehensive Analysis and General Economic-Environmental Evaluation of Cooling Techniques for Photovoltaic Panels – Part I: Passive Cooling Techniques, *Energy Convers. Manag., 149* (2017), Oct., pp. 334-354
[8] Andjelkovic, A. S., *et al.*, Development of Simple Calculation Model for Energy Performance of Double Skin Façades, *Thermal Science, 16* (2012), Suppl. 1, pp. S251-S267
[9] Clarke, J. A., *Energy Simulation in Building Design*, Butterworth-Heinemann, Oxford, UK, 1985
[10] ***, EnergyPlus V8.7 Engineering Reference, U. S. Department of Energy, 2016
[11] Charron, R., Athienitis, A. K. K., Optimization of the Performance of Double-Façades with Integrated Photovoltaic Panels and Motorized Blinds, *Sol. Energy*., *80* (2006), 5, pp. 482-491
[12] Bahrenbrug, A., *Psychrometry and Psychrometric Charts*, Cape and Transvaal Printers Ltd., Cape Town, South Africa, 1974
[13] Bazilian, M. D., *et al.*, Thermographic Analysis of a Building Integrated Photovoltaic System, *Renew. Energy*., *26* (2002), 3, pp. 449-461
[14] Palyvos, J. A., A Survey of Wind Convection Coefficient Correlations for Building Envelope Energy Systems' Modeling, *Appl. Therm. Eng., 28* (2008), 8-9, pp. 801-808
[15] Charron, R., Athienitis, A. K., A Two-Dimensional Model of a Double-Façade with Integrated Photovoltaic Panels, *J. Sol. Energy Eng. Trans. ASME*, *128* (2006), 2, pp. 160-167
[16] Bejan, A., *Convection Heat Transfer*, Jonh Wiley and Sons, New York, USA, 2013
[17] Saelens, D., Energy Performance Assessment of Single Storey Multiple-Skin Façades, Katholieke Universiteit Leuven, Leuven, Belgium, 2002
[18] Rohsenow, W. M., *et al.*, *Handbook of Heat Transfer Fundamentals*, McGraw-Hill, New York, USA, 1985
[19] Stazi, F., *et al.*, Experimental Evaluation of Ventilated Walls with an External Clay Cladding, *Renew. Energy*, *36* (2011), 12, pp. 3373-385
[20] Cengel, *Heat & Mass Transfer: A Practical Approach*, McGraw-Hill Education (India) Pvt Limited, New York, USA, 2007
[21] Kreith, F., *CRC Handbook of Thermal Engineering*, CRC Press, Boca Raton, Fla., USA, 1999
[22] Rohsenow, W. M., *et al.*, *Handbook of Heat Transfer*, McGraw-Hill, New York, USA, 1998
[23] White, F. M., *Fluid Mechanics*, McGraw Hill, New York, USA, 2011
[24] ***, ASHRAE, Handbook Fundamentals, *American Society of Heating, Air-Conditioning and Refrigeration Engineers*, Inc., 2013
[25] Townsend, T. U., A Method for Estimating the Long-Term Performance of Direct-Coupled Photovoltaic Systems, Univercity of Wisconsin, Madison, Vis., USA, 1989
[26] Kunz, W. A. G., Internal Series Resistance Determinated of Only One IV-Curve under Illumination, in: *Proceedings*, 19th Eur. Photovolt. Sol. Energy Conf., Paris, 2004
[27] Widalys, D. S., Improvement and Validation of a Model for Photovoltaic Array Performance, *Solar Energy*, *80* (2006), 1, pp. 78-88

Paper submitted: September 5, 2017
Paper revised: October 23, 2017
Paper accepted: October 27, 2017